Electronic Supplementary Material (ESI) for Journal of Materials Chemistry A.

Electronic Supplementary Information (ESI)

Confined Growth of MOF Nanocrystals by "Locked" Metal Ion Source

Zhongliang Huang,[a] LongLong Fan,[a] Bin Chen,[a] Shu-feng Zhou,[a] Jiale Huang,[b] Qingbiao Li,[b,c] and Guowu Zhan[a,*]

[a] College of Chemical Engineering, Integrated Nanocatalysts Institute (INCI), Huaqiao University, 668 Jimei Avenue, Xiamen, Fujian, 361021, P. R. China

[b] Department of Chemical and Biochemical Engineering, College of Chemistry and Chemical Engineering, Xiamen University, 422 South Siming Road, Xiamen, Fujian, 361005, P. R. China

[c] College of Food and Biology Engineering, Jimei University, 185 Yinjiang Road, Xiamen, Fujian 361021, P. R. China

*E-mail: gwzhan@hqu.edu.cn (G. Zhan)

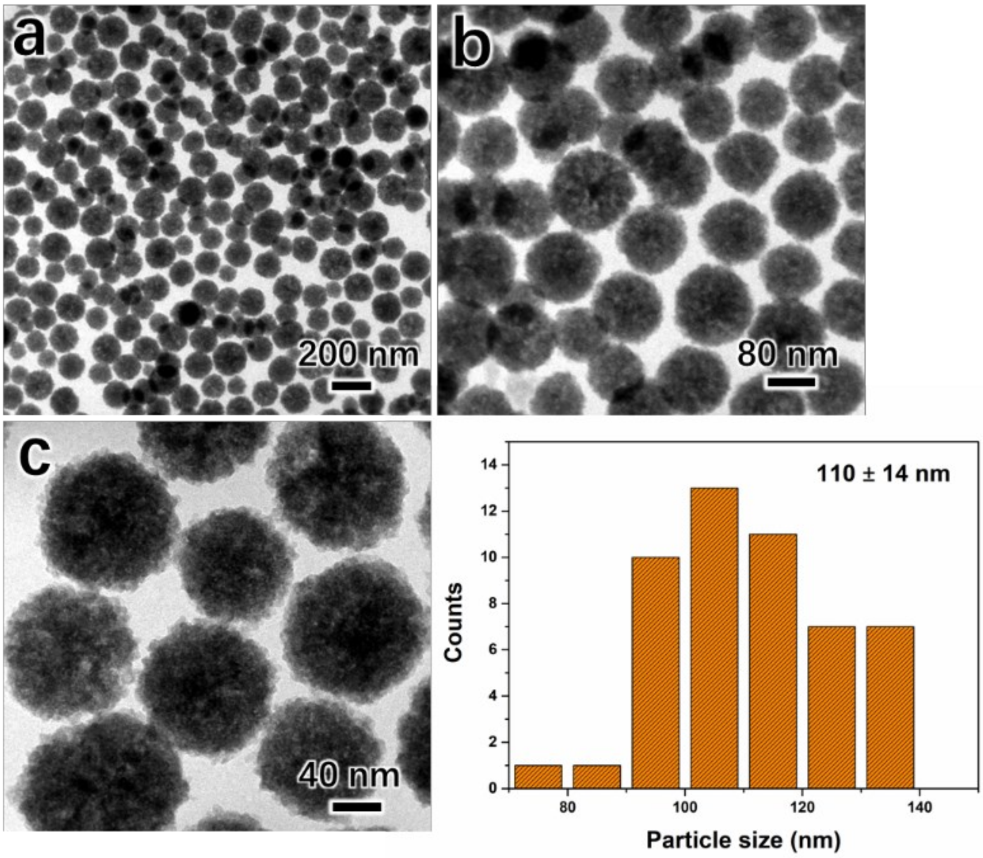

Figure S1. (a-c) Representative TEM images (at different magnifications) of Cu_2O nanoparticles, and (d) size distribution histograms of the Cu_2O nanoparticles.

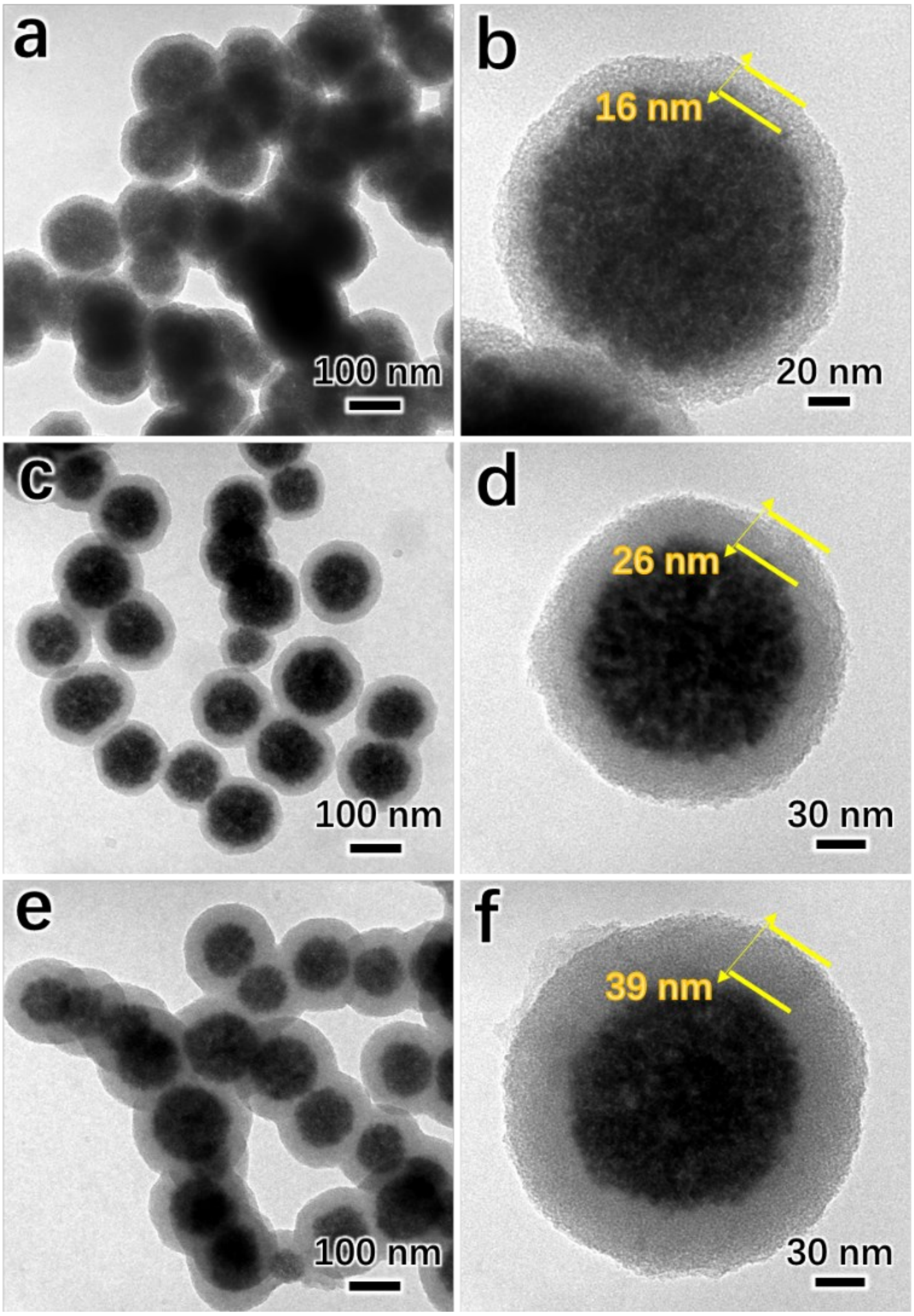

Figure S2. Representative TEM images (at different magnifications) of $Cu_2O@\textit{m}SiO_2$ with different coating thicknesses. (a, b) 16 nm, (c, d) 26 nm, and (e, f) 39 nm.

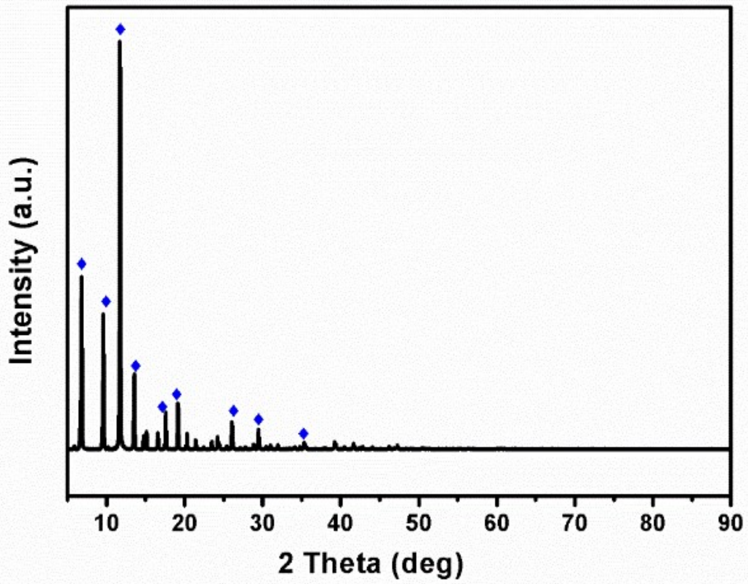

Figure S3. XRD pattern of MOF@*m*SiO_2 product prepared by mixing Cu_2O@*m*SiO_2 with H_3BTC ethanolic solution. The blue-color rhombus represents the characteristic diffraction peaks of the HKUST-1 phase.

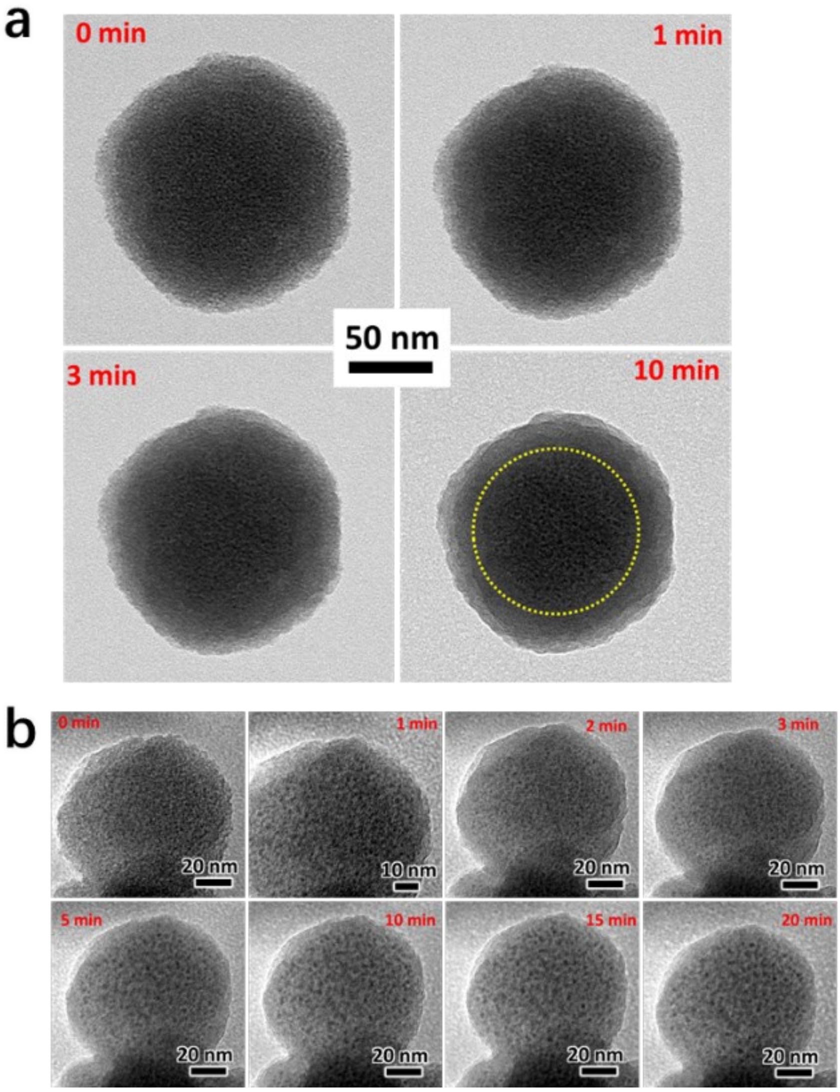

Figure S4. (a, b) The morphology changes of two MOF@*m*SiO_2 particles due to the degradation of the MOF structure under the irradiation of the high-energy electron beam (during the TEM observation).

Comments: As shown, the samples were sensitive to TEM electron beam imaging. The electron-beam induced the morphology change. It was found that the electron beam illumination led to the reduction of copper in HKUST-1 under high vacuum conditions, which showed a distinguished boundary between the MOF in the core and the silica in the shell after electron beam illumination for 10 min.

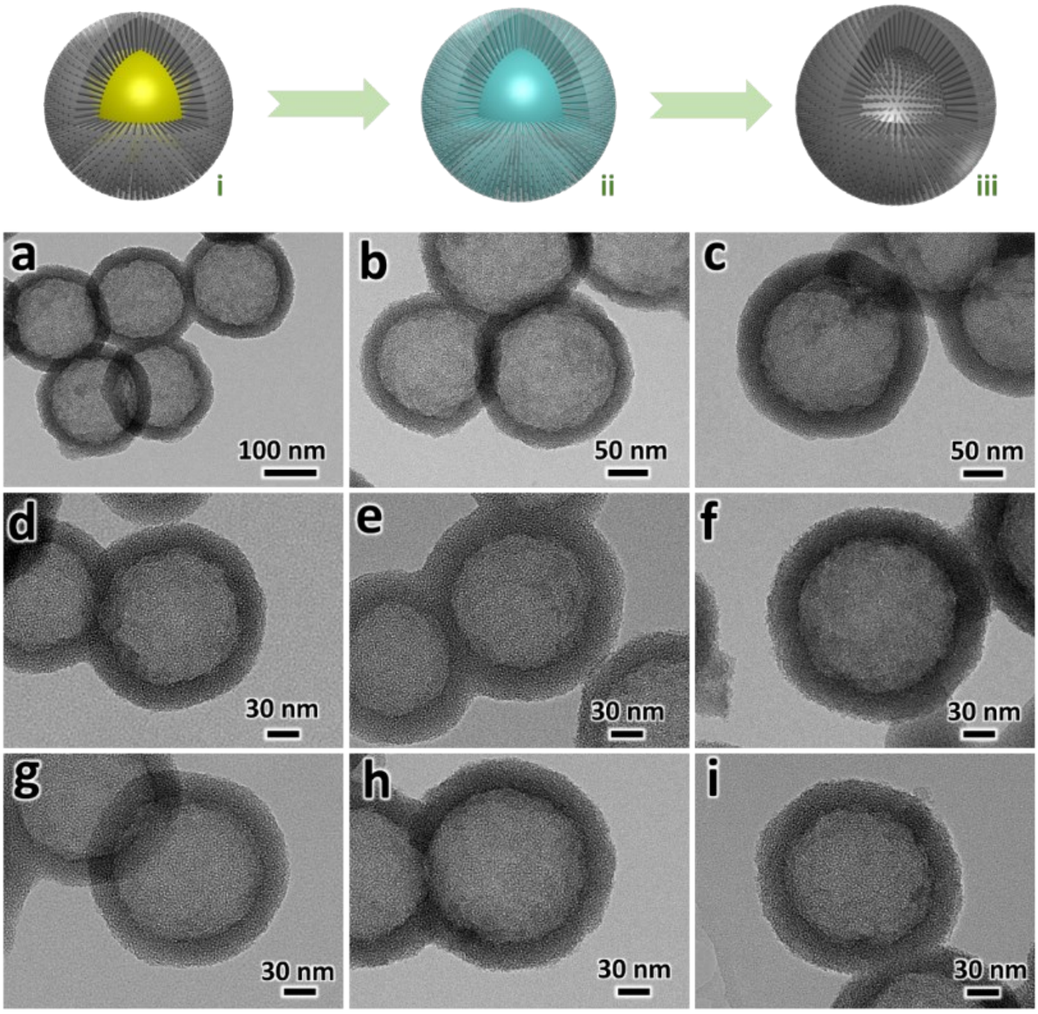

Figure S5. (a-i) TEM images (at different magnifications) of the product from the treatment of core-shell structured MOF@*m*SiO_2 with 15 mL of water for 12 h (under vigorously stirring). Model (i) represents core-shell structured Cu_2O@*m*SiO_2, model (ii) represents core-shell structured MOF@*m*SiO_2, and model (iii) represents the hollow silica shell.

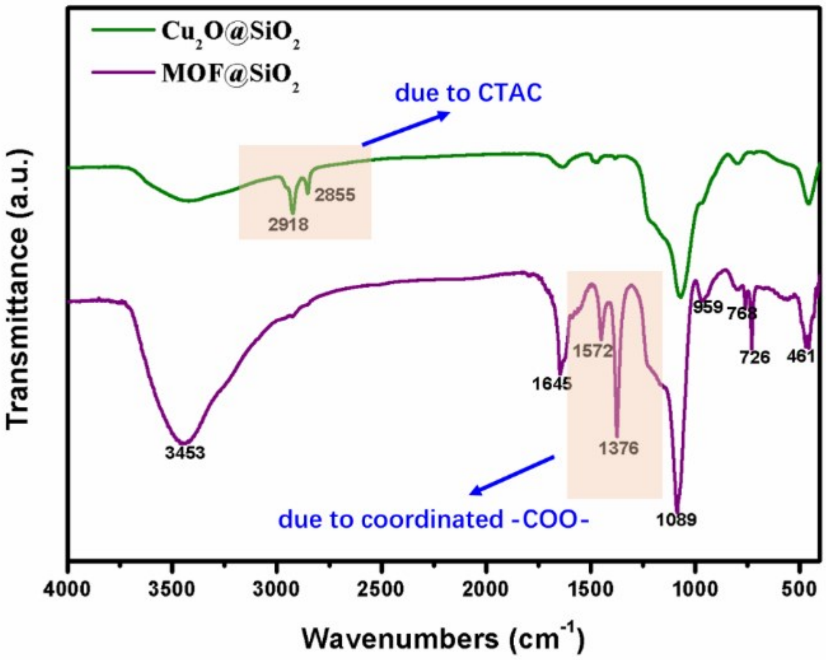

Figure S6. FTIR spectra of $Cu_2O@m SiO_2$ and $MOF@m SiO_2$ samples.

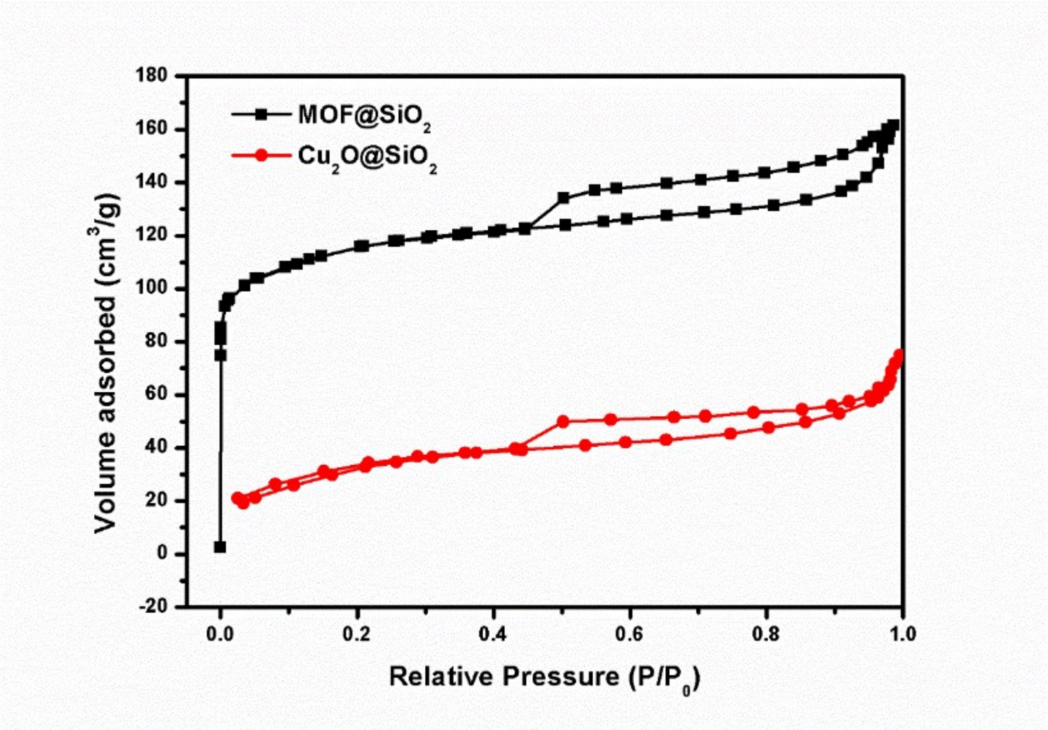

Figure S7. The N_2 physisorption isotherms of Cu_2O@*m*SiO_2 and MOF@*m*SiO_2 samples.

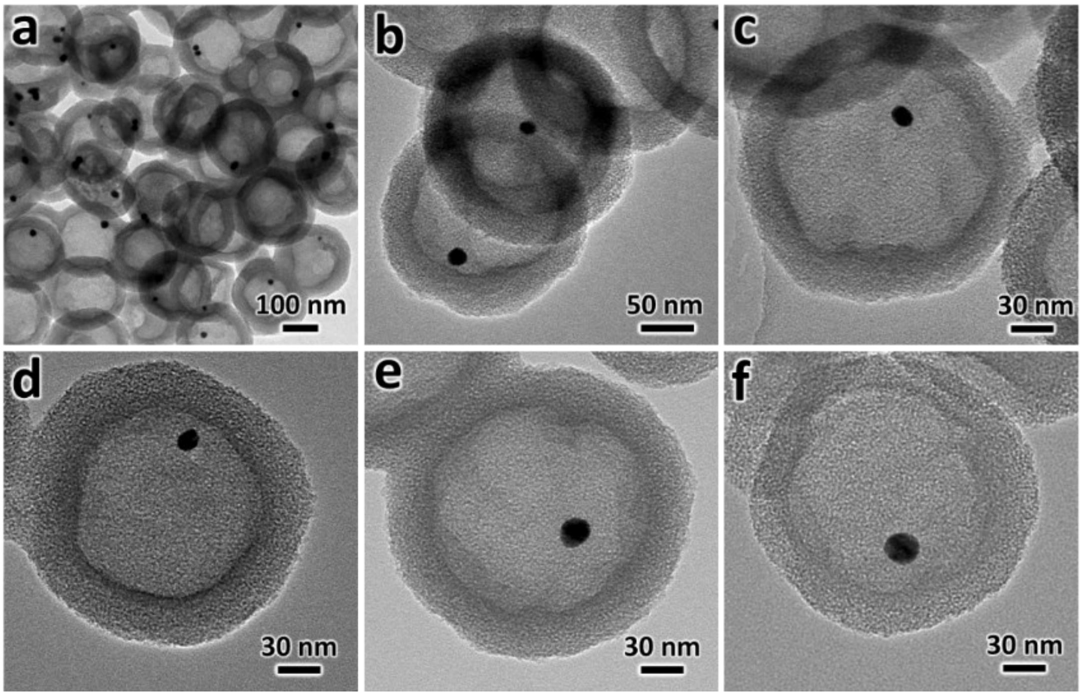

Figure S8. TEM images of the product after soaking Au@MOF@mSiO$_2$ in water for 12 h.

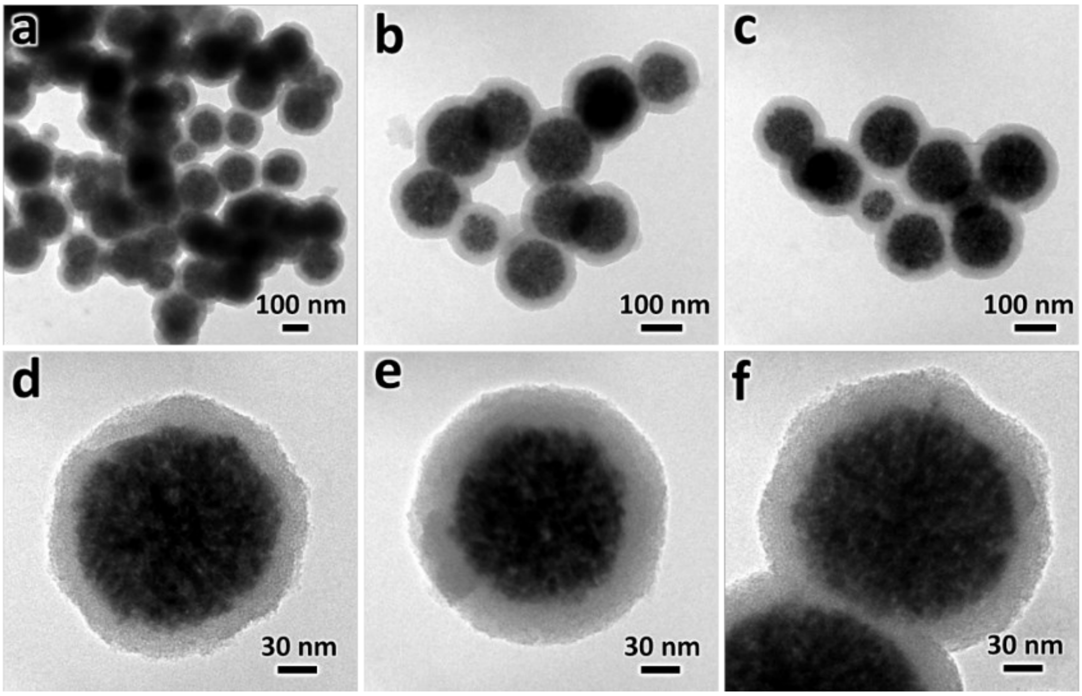

Figure S9. (a-f) TEM images (at different magnifications) of the product without the addition of H_3BTC during the transformation process.

Comments: Experimental condition: 2 mL of $Cu_2O@m\mathrm{SiO}_2$ suspension was mixed with 13 mL of pure ethanol, and the mixture was hydrothermally treated at 120°C for 12 h.

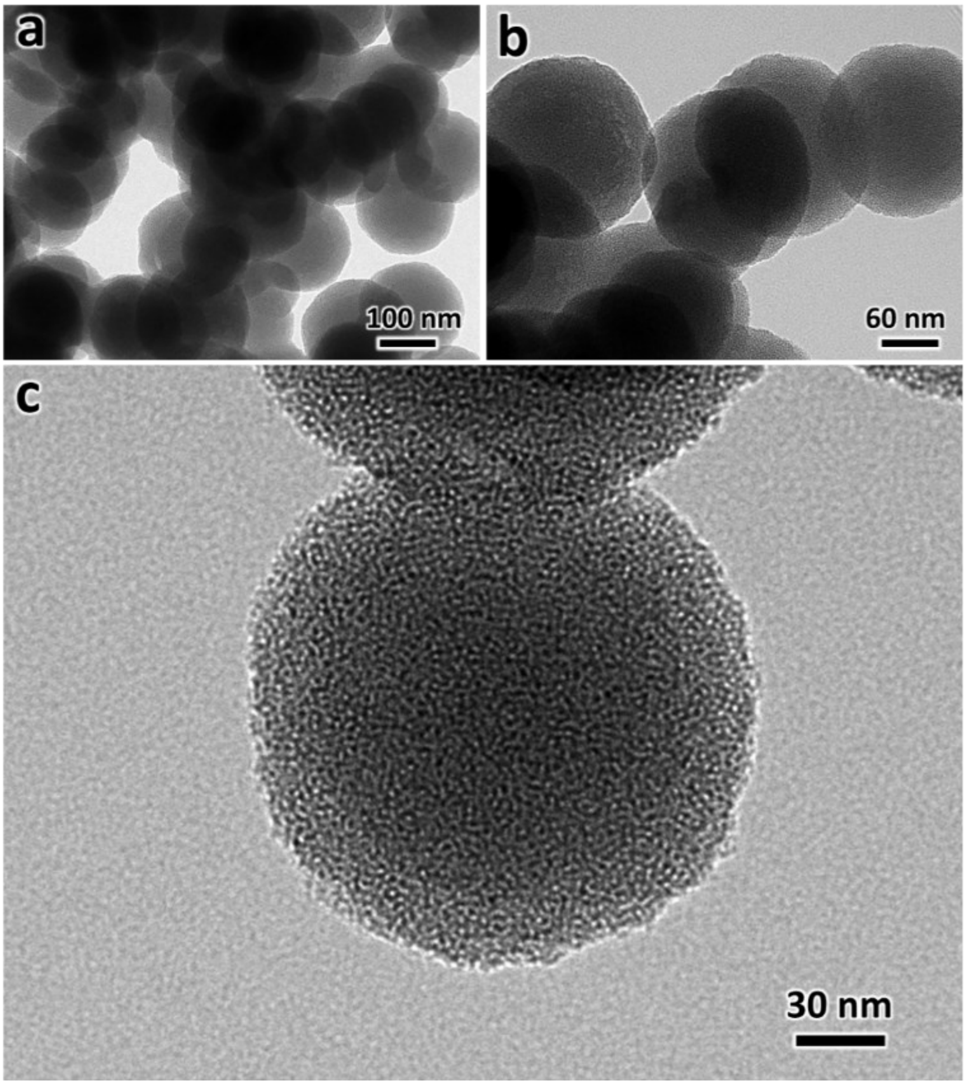

Figure S10. TEM images (at different magnifications) of the product obtained at H_3BTC concentration of 105 mM.

Comments: The effect of H_3BTC concentration on the formation of HKUST-1 inside silica shell was investigated. Herein, the concentration of H_3BTC was adjusted to 60 mM, 105 mM, 121 mM, 136 mM, 151 mM, and 196 mM, respectively, as 4 mL, 7 mL, 8 mL, 9 mL, 10 mL, and 13 mL of H_3BTC stock solution (0.226 M) was used during the synthesis. For this experiment: 2 mL of $Cu_2O@m SiO_2$ was mixed with 7 mL of H_3BTC ethanolic solution (0.226 M) and 6 mL of pure ethanol. Afterward, the mixture was hydrothermally treated at 120^{o}C for 12 h.

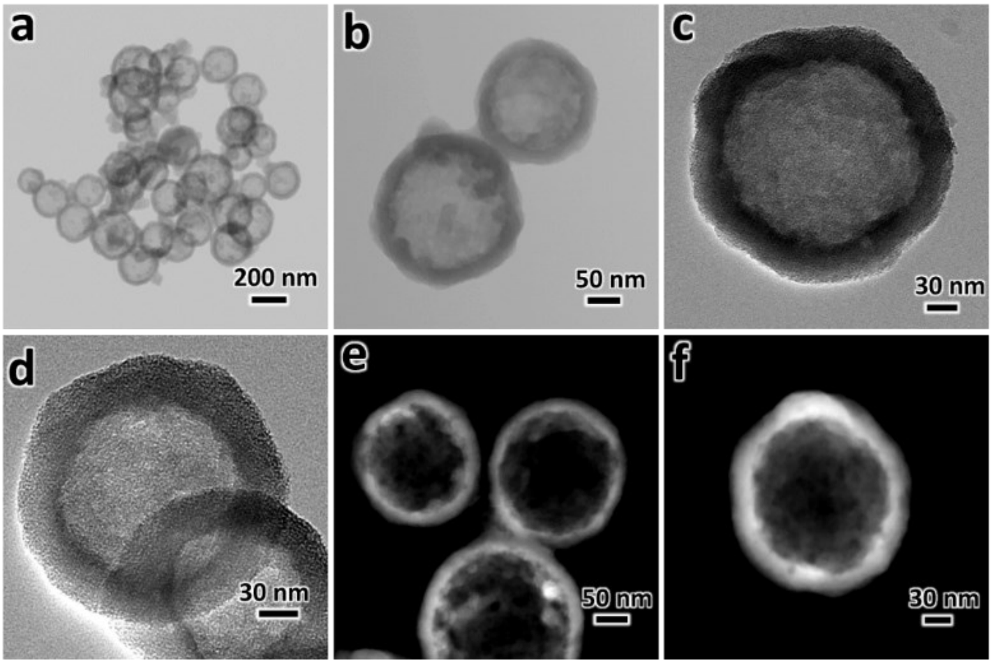

Figure S11. TEM images and HAADF-STEM images of the product obtained at a high concentration of H_3BTC of 196 mM.

Experimental conditions: 2 mL of $Cu_2O@m SiO_2$ ethanolic suspension was mixed with 13 mL of H_3BTC ethanolic solution (0.226 M). Afterward, the mixture was hydrothermally treated at 120^{o}C for 12 h.

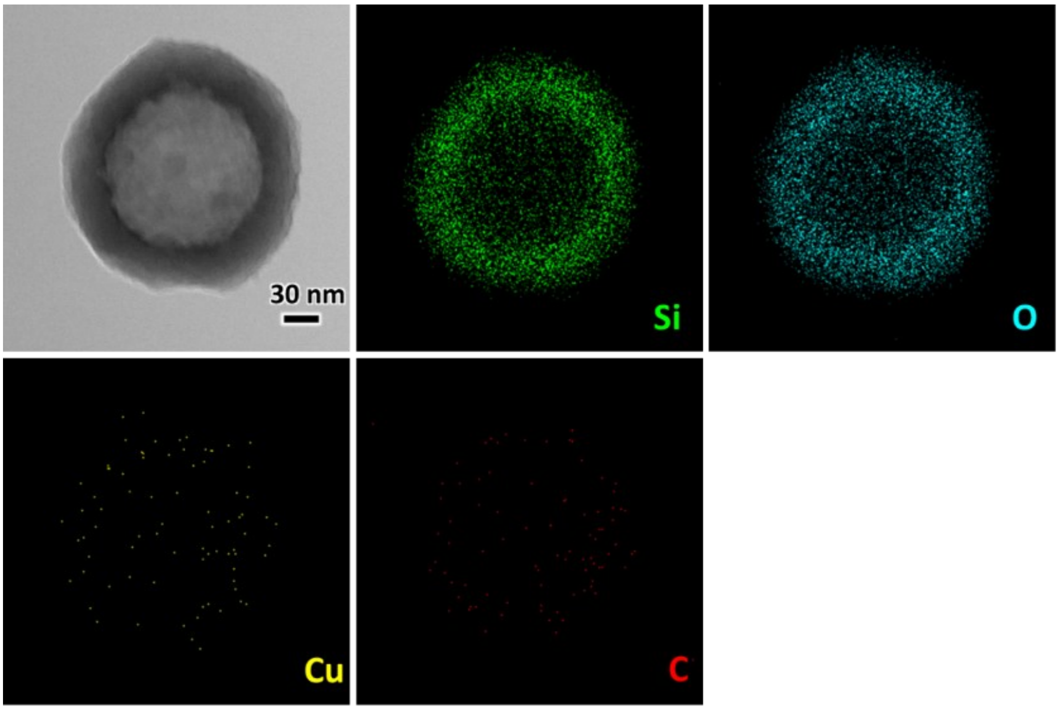

Figure S12. EDX elemental maps of the product synthesized at a high concentration of H_3BTC (196 mM).

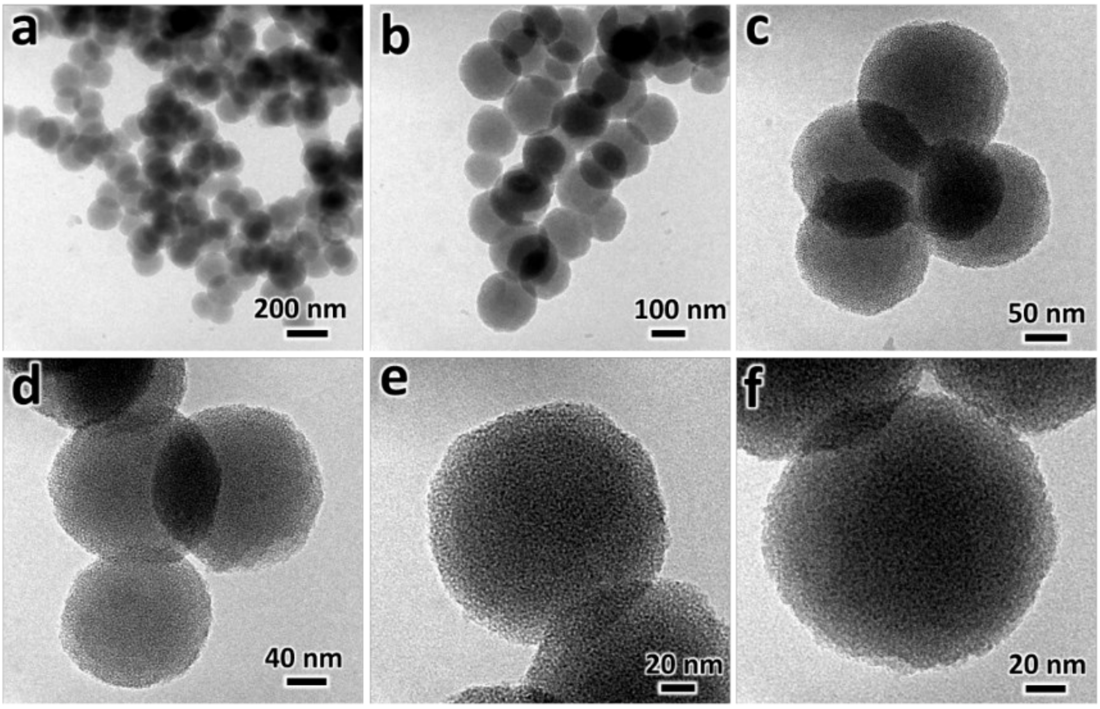

Figure S13. Formation of core-shell structured HKUST-1@mSiO$_2$ by using Cu$_2$O@mSiO$_2$ with a thinner silica coating layer (16 nm) as a template. (a-f) TEM images at different magnifications.

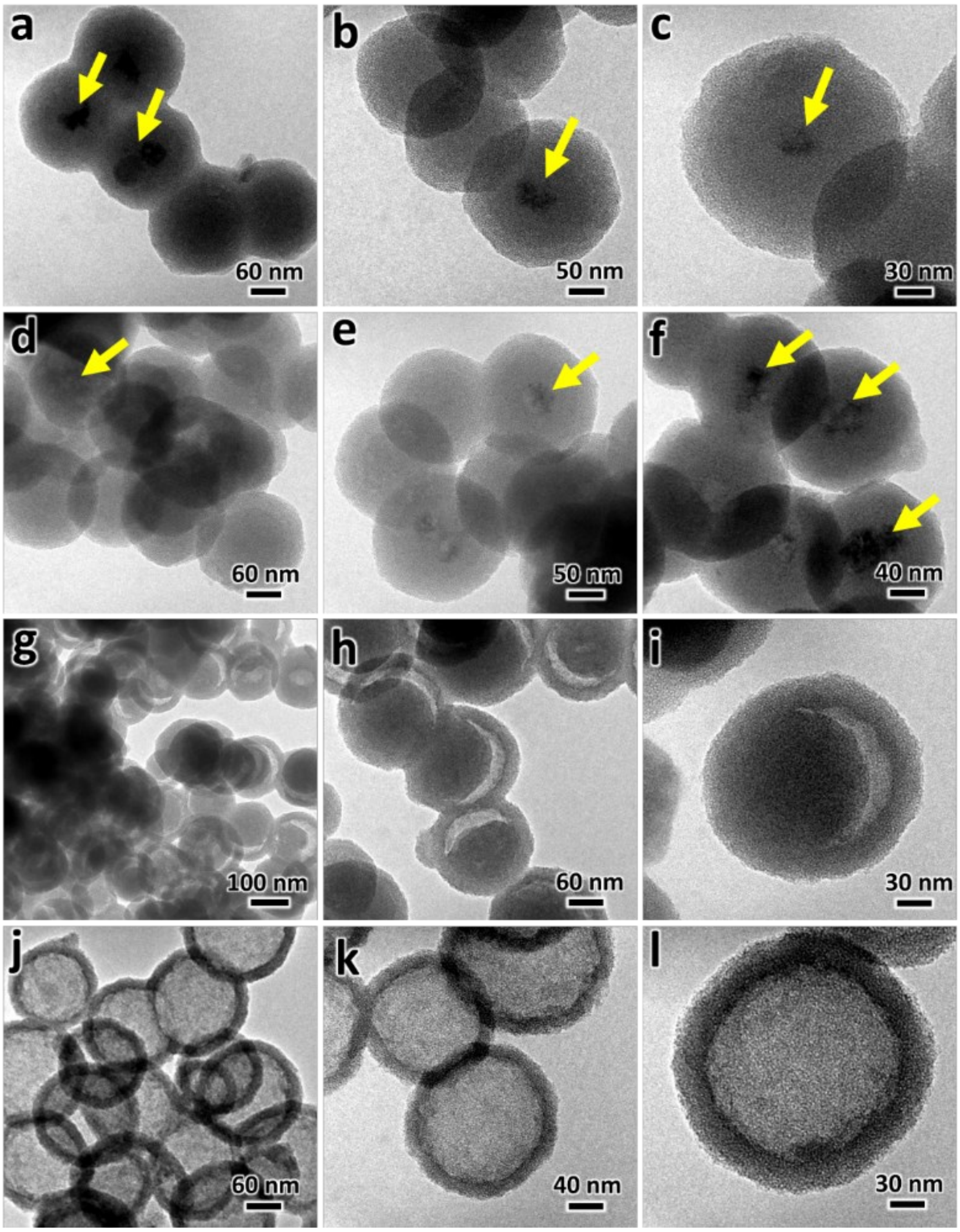

Figure S14. TEM images (at different magnifications) of the products prepared at the different reaction temperatures. (a-c) 60°C, (d-f) 80°C, (g-i) 160°C, and (j-l) 180°C. The yellow arrows show the unreacted Cu_2O.

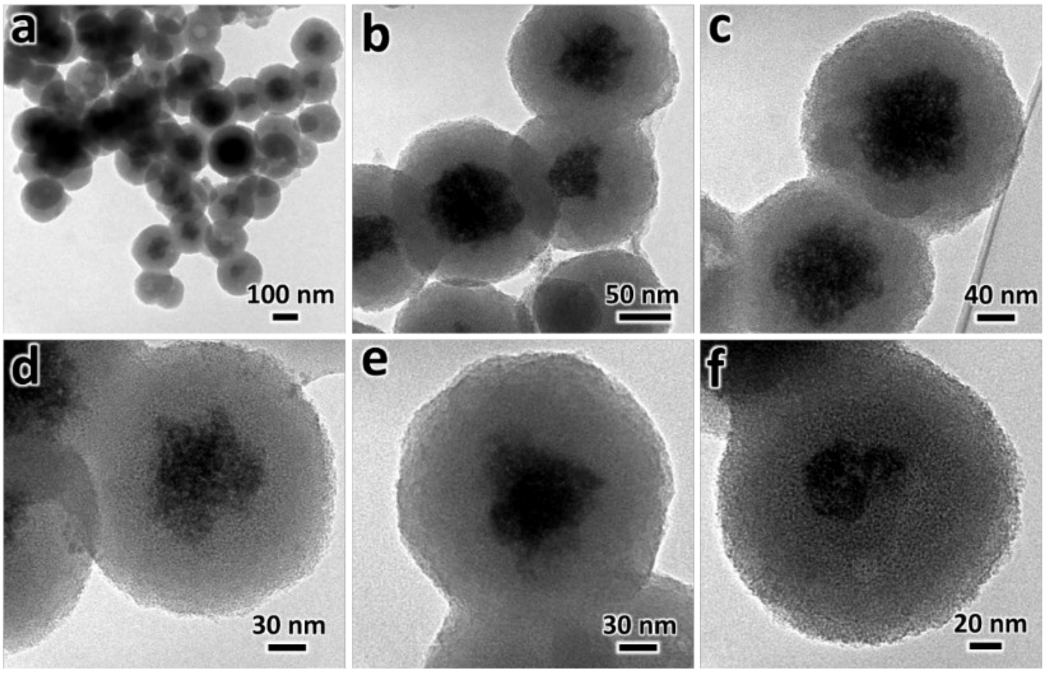

Figure S15. (a-f) TEM images (at different magnifications) of the product obtained in the initial stage of the reaction (0.5 h).

Comment: As shown, at the reaction time of 0.5 h, the products were not fully developed with the residual Cu_2O in the core portion of the composites.

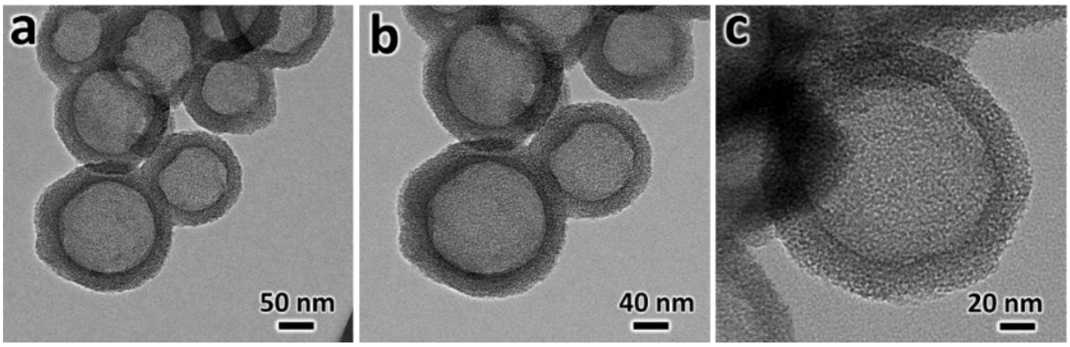

Figure S16. The transformation of $Cu_2O@m\mathrm{SiO}_2$ in the DMF solvent (9 mL) at 120°C for 12 h.

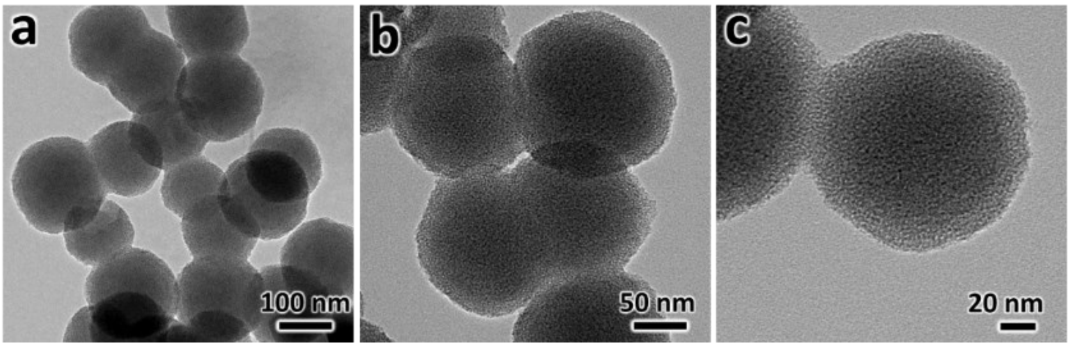

Figure S17. The transformation of $Cu_2O@mSiO_2$ in the methanol solvent (9 mL) at 120^{o}C for 12 h.

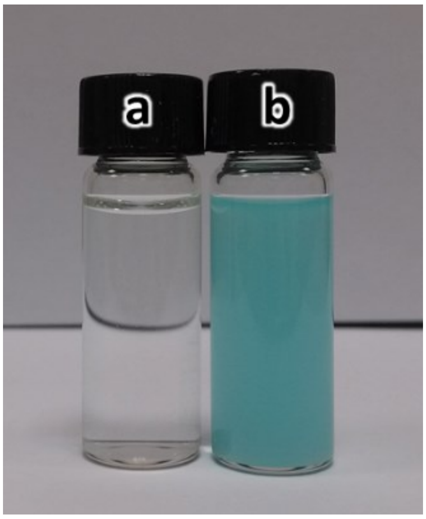

Figure S18. The transformation of $Cu_2O@m SiO_2$ in the water solvent (9 mL) at 120^{o}C for 12 h. (a) the photography of the product, and (b) the photography of the comparison sample by using ethanol as solvent.

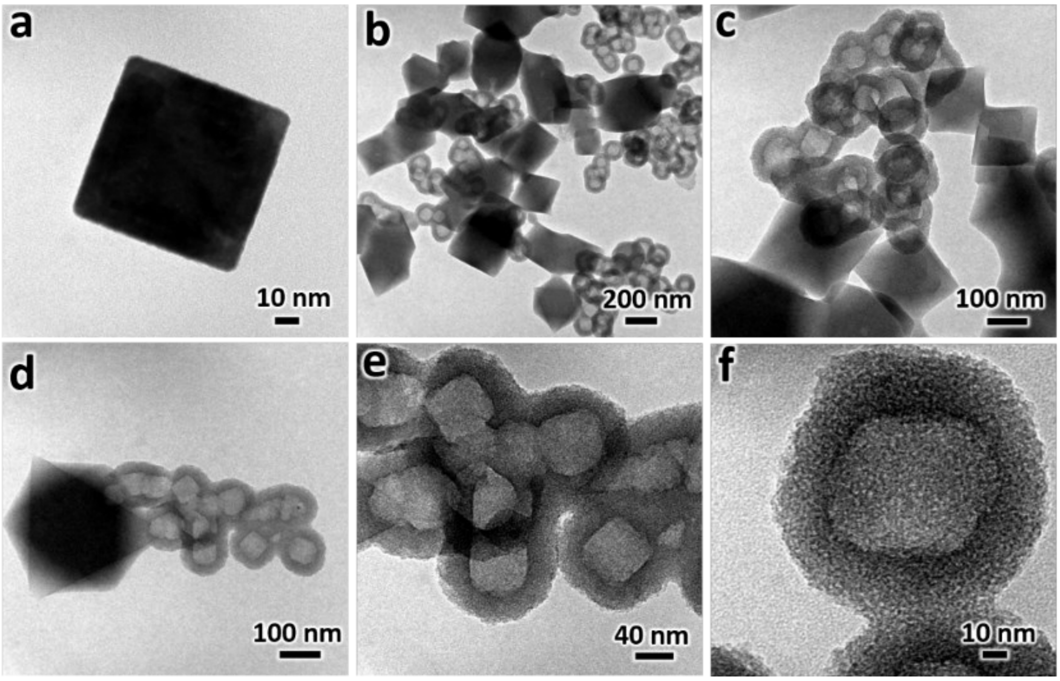

Figure S19. (a) TEM image of the cubic Cu_2O, and (b-f) TEM images of the products by the transformation of cubic $Cu_2O@m SiO_2$ as mixing with H_3BTC ethanolic solution at 120°C for 12 h.

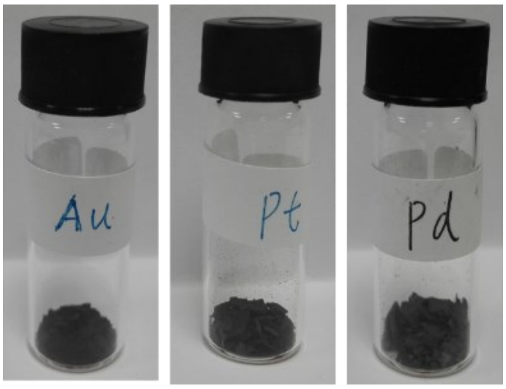

Figure S20. Digital photos of the three different (MNP/MOF)@$m\mathrm{SiO_2}$ composites.

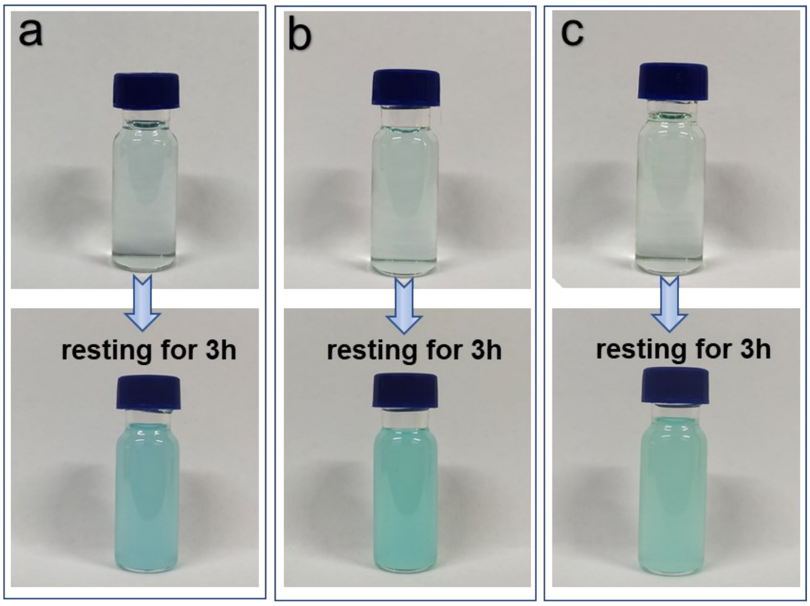

(Au/MOF)@mSiO$_2$ (Pt/MOF)@mSiO$_2$ (Pd/MOF)@mSiO$_2$

Figure S21. Digital photos of the supernatant solution from the synthesis solutions of MNP/MOF@mSiO$_2$ composites after centrifugation.

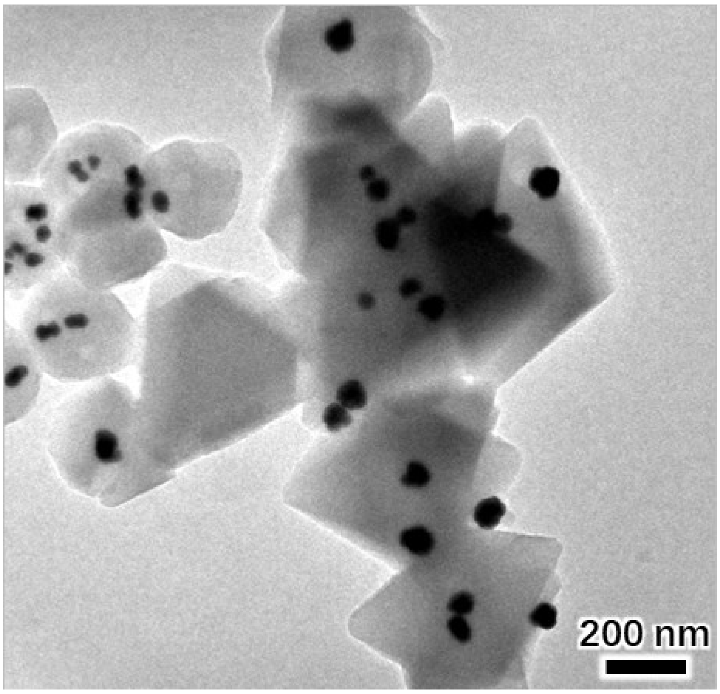

Figure S22. TEM image of the product obtained by directly mixing $HAuCl_4$/H_3BTC with Cu_2O@*m*SiO_2 at an extended reaction time (30 min).

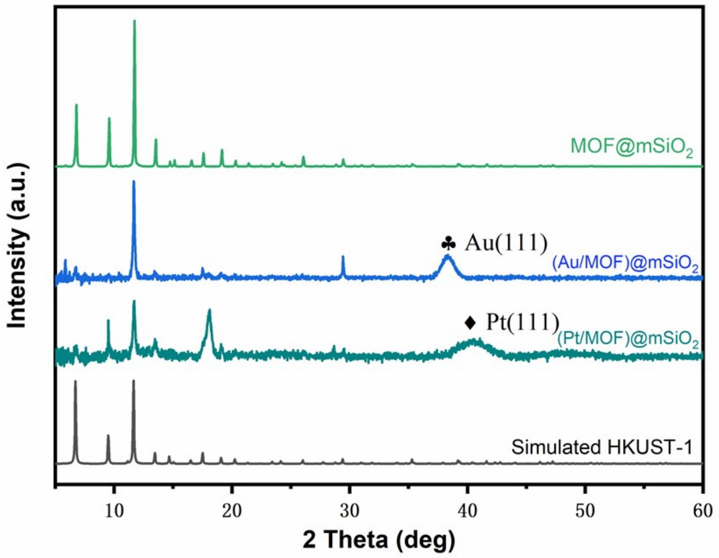

Figure S23. XRD patterns of MOF@*m*SiO$_2$, (Au/MOF)@*m*SiO$_2$, (Pt/MOF)@*m*SiO$_2$, and the simulated HKUST-1.

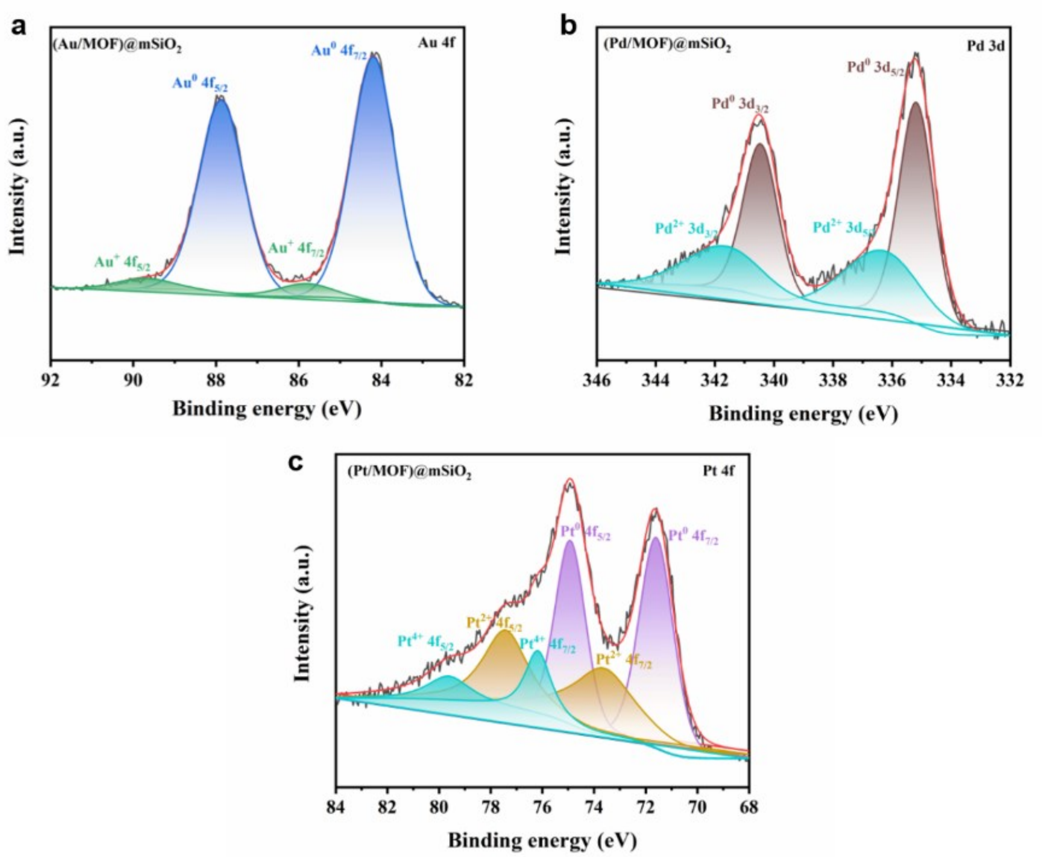

Figure S24. (a) Au 4f, (b) Pd 3d, and (c) Pt 4f XPS spectra of the (Au/MOF)@*m*SiO$_2$, (Pd/MOF)@*m*SiO$_2$, and (Pt/MOF)@*m*SiO$_2$ catalysts.

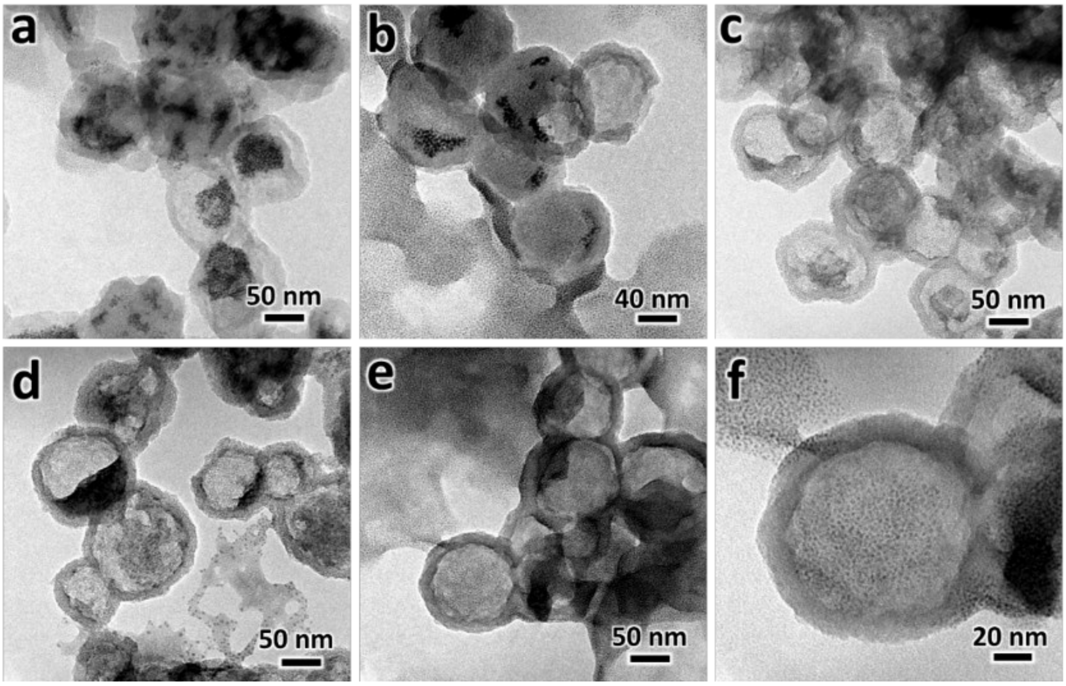

Figure S25. TEM images of the products prepared by applying surfactant during the growth of AuNPs. (a, b) 30 μL of 1-propanethiol, (c, d) 30 μL of 3-mercaptopropionic acid, and (e, f) 30 μL of 1-dodecanethiol. Reaction temperature: room temperature.

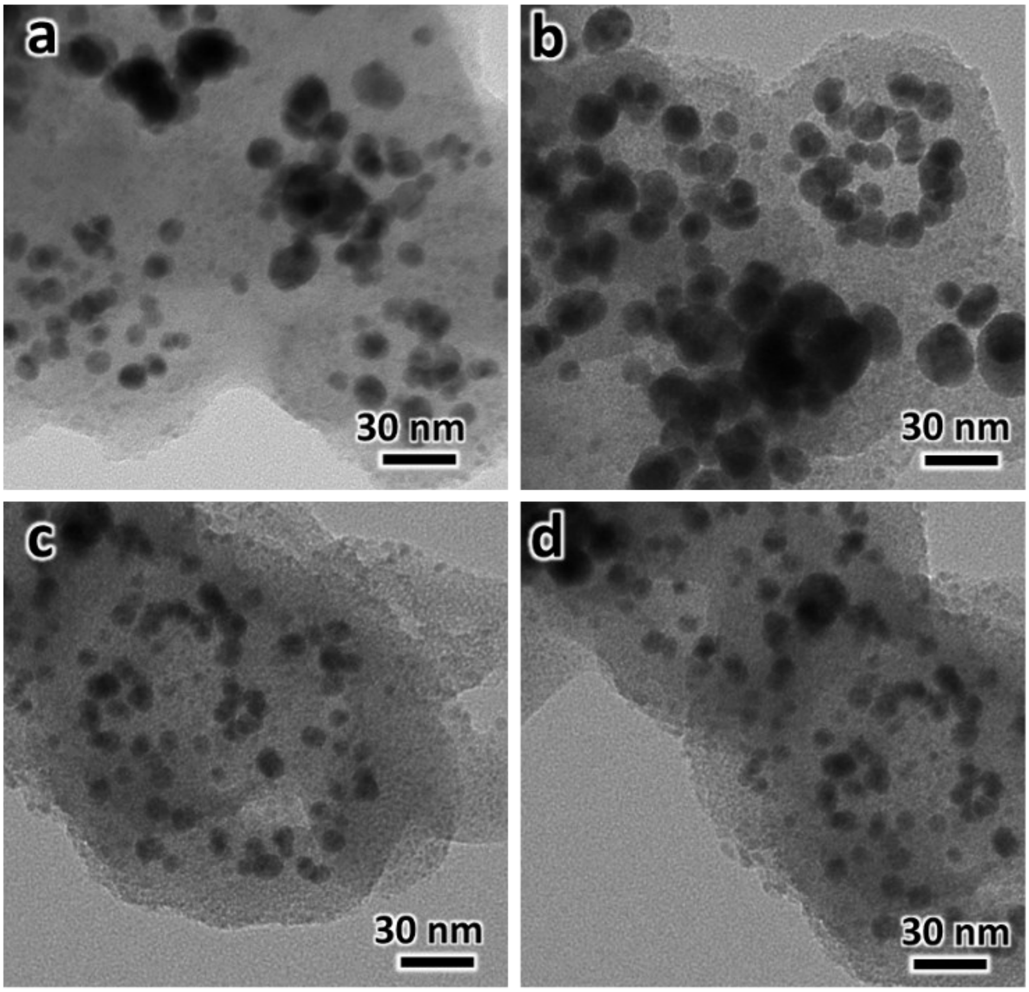

Figure S26. TEM images of the spent Au/MOF@*m*SiO$_2$ catalyst after the benzyl alcohol oxidation reaction at 90^{o}C for 6 h.

Table S1 Catalytic performance of various catalysts for CO oxidation reaction.

MNP/MOF	Space velocity (mL/g/h)	T_{100} (°C)	Reference
Au/ZIF-8	60000	314-314	[1]
Au/UiO-66	15000	240	[2]
Pd/Cu-BTC	24000	220	[3]
Pt/UiO-67	120000	380~490	[4]
Pd/Cu-BTC	120000	240	[5]
Pt/MIL-101	24000	277	[6]
Ag/Cu-BTC	24000	122	[7]
Pt/MIL-101	20000	150	[8]
PtNi/UiO-67	120000	180	[9]
Pd/Ce-MOF	24000	92~190	[10]
Au/HKUST-1@*m*SiO_2	8571	205	this work
Pt/HKUST-1@*m*SiO_2	8571	230	this work
Pd/HKUST-1@*m*SiO_2	8571	240	this work

References

1. H.-L. Jiang, B. Liu, T. Akita, M. Haruta, H. Sakurai and Q. Xu, *Journal of the American Chemical Society*, 2009, **131**, 11302-11303.
2. R. Wu, X. Qian, K. Zhou, H. Liu, B. Yadian, J. Wei, H. Zhu and Y. Huang, *Journal of Materials Chemistry A*, 2013, **1**, 14294-14299.
3. J.-y. Ye and C.-j. Liu, *Chemical Communications*, 2011, **47**, 2167-2169.
4. R. Vakili, E. K. Gibson, S. Chansai, S. Xu, N. Al-Janabi, P. P. Wells, C. Hardacre, A. Walton and X. Fan, *ChemCatChem*, 2018, **10**, 4238-4242.
5. F. Abbasi, J. Karimi-Sabet and C. Ghotbi, *International Journal of Hydrogen Energy*, 2020, **45**, 21450-21463.
6. E. V. Ramos-Fernandez, C. Pieters, B. van der Linden, J. Juan-Alcañiz, P. Serra-Crespo, M. W. G. M. Verhoeven, H. Niemantsverdriet, J. Gascon and F. Kapteijn, *Journal of Catalysis*, 2012, **289**, 42-52.
7. Y. Zhao, C. Zhong and C.-J. Liu, *Catalysis Communications*, 2013, **38**, 74-76.
8. A. Aijaz, A. Karkamkar, Y. J. Choi, N. Tsumori, E. Rönnebro, T. Autrey, H. Shioyama and Q. Xu, *Journal of the American Chemical Society*, 2012, **134**, 13926-13929.
9. R. Vakili, T. J. A. Slater, C. Hardacre, A. S. Walton and X. Fan, *Journal of Catalysis*, 2020, **391**, 522-529.
10. A. Lin, A. A. Ibrahim, P. Arab, H. M. El-Kaderi and M. S. El-Shall, *ACS Applied Materials & Interfaces*, 2017, **9**, 17961-17968.